ARTICLE

Visualization on the Behavior of Inert Gas Jets Impinging on a Single Glass Tube Submerged in Liquid Sodium

Hideyuki Kudoh[a,*], Ken-ichiro Sugiyama[a], Tadashi Narabayashi[a],

Hiroyuki Ohshima[b], and Akikazu Kurihara[b]

[a] *Hokkaido University, North 13 West 8, Kita-ku, Sapporo 060-8628, Japan;* [b] *Japna Atomic Energy Agency, Narita, O-arai-machi, Ibaraki 311-1393, Japan*

(Received)

In order to accurately model sodium–water reaction jets in steam generators of fast breeder reactors, knowledge of size distributions or mean diameters of liquid sodium droplets entrained into the reaction jets are prerequisite. In the present study, argon-gas jet behaviors, without chemical reaction, injected into liquid sodium were successfully visualized using an endoscope and a glass tube, and the size distributions and mean diameters of liquid sodium droplets entrained into the gas jet were also obtained in the bubbling regime.

Most of the liquid sodium droplets were observed to be intermittently produced in the vicinity of a gas nozzle in the present study. The droplet size distributions of entrained sodium droplets were found to agree well with the Nukiyama–Tanasawa distribution function when the arithmetic mean diameter was used. The Sauter mean diameters obtained in the present study were also found to be well correlated with an empirical equation proposed by Epstein *et al.*. The present study shows that the existing knowledge, which is based on the results of

[*]Corresponding author, E-mail: k.hide.16@eng.hokudai.ac.jp

water experiments, is suitable in terms of accuracy in practice.

KEYWORDS: liquid sodium, submerged gas jet, visualization, droplet size distribution, mean droplet diameter, sodium-water reaction, fast breeder reactor

1. Introduction

When a heat transfer tube in a steam generator of a sodium-cooled fast breeder reactor causes a leak of high-pressure water or steam into surrounding liquid sodium, secondary failures of adjacent heat transfer tubes are expected, due to the high-temperature and highly corrosive reaction jet originating from fine sodium droplets that are numerously entrained into the leak jet. Therefore, the understanding of the mechanisms of the entrainment of sodium and the generation of sodium droplets, in addition to the prediction of the droplet size distributions, are prerequisite in order to accurately model and predict the peak temperature in this type of reaction jet. However, even experimental investigations for gas jets injected into liquid sodium without chemical reaction have not yet been conducted.

For void fraction measurements directly related to water droplets entrained into submerged gas jets, Loth and Feath measured the local void fraction distribution and static pressure distribution of underexpanded jets submerged in water [1, 2]. Bell *et al.* also measured the void fraction distribution of submerged impinging jets [3]. Someya *et al.* investigated the spread angle of submerged gas jets and the velocity distribution of ambient water using their own visualization method [4]. For the mean diameters of entrained water droplets, Epstein *et al.* proposed the empirical correlation between the dimensionless Sauter mean diameter and the Weber number using results of water droplets, which were produced in the immediate vicinity of the nozzle exit in very shallowly submerged gas jets [5]. However, there have been no studies measuring droplet size or number for liquid sodium entrained in gas jets. Moreover, there have been no studies observing the droplets of liquid sodium entrained into high-velocity gas jets injected in liquid sodium. Therefore, experimental investigations using liquid sodium are required in order to clarify phenomena in sodium-entrained jets and ensure the availability of the existing data of water-entrained jets.

The objective of the present experimental study is to understand the process of droplet generation from liquid sodium entrained into high-velocity gas jets injected in liquid sodium

and to measure the sodium droplet size and number. A technique for visualizing gas jets impinging on a single cylinder submerged in liquid sodium, the configuration of which corresponds to the simplest system in the reaction jets in steam generators, was first developed using a glass tube and an endoscope. Several observations performed using this technique were conducted in the "bubbling regime" covering the range of gas jet velocity up to 125 m/s at the nozzle exit, where gas jets were intermittently injected into liquid sodium as reported by Sano *et al.* [6]. In their paper, only the existence of a bubbling regime and a jetting regime in gas jets submerged in liquid mercury, which was found by direct observation from the nozzle side, was reported from the viewpoint of the steel industry.

In the present study, the authors found that most sodium droplets are produced in the vicinity of the gas nozzle. The droplet size distributions measured in the submerged gas jets of the present study were confirmed to agree well with the Nukiyama–Tanasawa correlation, which has been widely used in describing liquid atomization occurring in sprays [7]. The mean diameters of sodium droplets obtained in the present study were also revealed to agree well with the dimensionless correlation by Epstein *et al.*, as explained above.

2. Experimental Apparatus

In the present study, only the test section shown in **Figure 1** was replaced in the previous experimental equipment [8]. The new test section of the stainless-steel vessel has an inner diameter of 80 mm and a height of 700 mm. A glass tube of 19 mm in outer diameter, which simulates an adjacent heat transfer tube, was inserted horizontally into the test section at a height of 180 mm from the bottom. The glass tube was made of Pyrex, which is less corroded in low-temperature liquid sodium. The diameter of the nozzle-hole, which was formed using a drill, was 3.5 mm, and the distance between the nozzle exit and the forward stagnation point of the glass tube was 25 mm. These dimensions are the same as those in the previous study, and are selected for the simultaneous visualization of gas-jet behaviors in

water from the nozzle head to the wake area near the back side of the cylinder [8]. In the present study, simultaneous visualization of the gas-jet behaviors in sodium from the nozzle hole to the outer surface of the forward side of the cylinder with a sufficient spatial resolution is required. The test section was filled with stationary liquid sodium, and the liquid level was adjusted to 550 mm from the bottom. High-purity argon gas (99.999%) was injected upward from the nozzle. An endoscope (Borescope 88570DF, Karl Storz GmbH & Co. KG), which can be used to perform right-angle observations, was inserted inside the glass tube. Images of the gas jet behavior were captured by a high-speed camera at a frame rate of 2000 fps (Fastcam-512PCI model 32K, Photron Ltd.) connected to the endoscope. Three conductivity probes for void fraction measurement used in the previous paper were placed around the glass tube [8]. The liquid sodium and argon gas temperatures were both maintained at 120°C.

The gas jet velocities at the nozzle exit were chosen to be $13 < u_0 < 125$ m/s. The gas jet velocity was calculated using the following equation:

$$u_0 = \frac{Q}{\pi d_0^{\,2}/4}, \tag{1}$$

where Q is the volume flow rate of the gas jet. The volume flow rate was controlled by a mass flow controller (Mass Flow Controller model 8000 series, Kojima Instruments Inc.) installed in the upstream of a gas heater and was corrected for the temperature of the gas jet at the nozzle exit. The pressure difference between the sodium pressure (atmospheric pressure) and the stagnation pressure of the gas jet at u_0 = 125 m/s was calculated from the isentropic assumption as 20 kPa, which can be assumed as incompressible flow. Therefore, under the present experimental condition, the gas jet velocity can be expressed by Equation (1).

Based on observations, Mori *et al.* have reported that two flow regimes appear in gas jets submerged in mercury [6]. According to their paper, when the gas jet velocity is less than the sonic velocity, the jet is intermittently injected into the liquid metal and referred to the behavior in this regime as “bubbling”. In contrast, when the gas jet velocity exceeds the sonic

velocity, the submerged gas jets are continuously injected through the nozzle, and they referred to the behavior in this regime as “jetting”. In order to clearly observe gas jet behaviors and formation processes for droplets in liquid sodium, the bubbling regime was selected in the present visualization study. As we describe later herein, intermittently injected gas jets were observed within the range of the present gas jet velocities.

3. Results and Discussion

3.1. Optical Images

Figure 2 shows optical images captured by a high-speed camera via the endoscope at the minimum gas jet velocity of u_0 = 13 m/s. A bright (white) area at the upper part of each image appears because the source light, as shown in Figure 1, reflects at the inner surface of the glass tube. When the glass tube surface was covered with sodium film, a gray area was observed due to the optical reflection from the liquid sodium surface (0 ms). When the sodium film was swept away by the gas jet, a relatively dark image, where the gas nozzle can be observed, was obtained (10 ms). In the figure, the letters “B” indicate a boundary line between the gas jet and the ambient liquid sodium on the glass tube or on the upper surface of the nozzle. Since the upper surface of the gas nozzle that was placed 25 mm below the glass tube can be clearly observed, the space between the nozzle and the glass tube was confirmed to be filled by the gas jet (20 ms). The upper surface of the nozzle was then gradually covered with liquid sodium (30 ms). During this time period (20 to 30 ms), the optical reflection at the gas–liquid interface indicates that many surface waves, as shown by the area indicated by the fine, solid-line at 20 ms, appear due to the shear force between the gas jet and the ambient liquid sodium. When the nozzle exit was completely covered, the liquid sodium surface at the nozzle exit was pushed up by the gas pressure in the nozzle, and a rapid elevation of the surface was observed. In addition, the optical reflection due to the surface waves at the interface almost disappears (40 ms). After that, the glass tube surface was re-covered with

sodium (50 ms). These periodic motions were repeated in the range of low gas jet velocity.

3.2. Formation Process of Sodium Droplets

When the gas jet velocity, u_0, exceeds 50 m/s, a number of liquid droplets impinging on the glass tube surface were observed. A clear formation of liquid droplets was observed at the near region from the nozzle when the nozzle exit was covered by ambient liquid sodium. **Figure 3** shows a close-up of the nozzle exit observed in the gas jet at u_0 = 75 m/s. The nozzle exit and the nozzle upper surface can be seen at the left side of the image (0 ms). Here, the nozzle was somewhat blurred compared to Figure 2 because the camera focused on the outer surface of the glass tube in order to clearly observe the liquid droplets at the tube surface. The nozzle upper surface was gradually covered with liquid sodium, and the diameter of the gas jet was decreased. When the nozzle exit almost disappeared from the image, a number of droplets obviously appeared at the glass tube surface (2 ms). Just after the nozzle exit disappeared, relatively large droplets reached the surface (4 ms). This time delay may be attributed to the difference in velocity of the droplets.

Typical images of another formation process of droplets were obtained at the far region from the nozzle, as shown in **Figure 4**. Liquid sodium ligaments appeared in the gas jet region (0 ms) and were then broken up into numerous droplets at the tube surface (0.5 ms). However, note that over 95 % of the droplet formation observed in the present study occurred at the near region of the nozzle exit.

Figure 5(a) qualitatively shows a simple image for the droplet generation that occurred intermittently in a short time period in the vicinity of the nozzle, as explained in Figure 3. Considering that the velocity distribution of the gas jet in the injecting direction depends on the cross-sectional area of the gas jet, the relative velocity between the gas jet and the ambient liquid sodium reaches a maximum value when the jet diameter in the vicinity of the nozzle is approximately equal to the nozzle diameter. Therefore, sodium droplets are

considered to have been produced by liquid sodium shearing off from the unstable gas–liquid interface that formed just above the nozzle exit due to the momentum exchange between the gas jet and the ambient liquid. Figure 5(b) explains the mechanism of droplet formation at the far region from the nozzle, as shown in Figure 4. The gas–liquid interface at the submerged gas jet causes numerous surface waves, as shown in the images at 20 to 30 ms in Figure 2, and highly rolled-up waves are generated with increasing gas jet velocity. The crests of the rolled-up waves are then entrained into the gas jet and form liquid ligaments. Liquid droplets are then produced by the disintegration of the liquid ligaments.

3.3. Area Average Void Fraction

Figure 6 shows a time series of the area average void fraction, α_a, measured at the forward stagnation area of the glass tube. The area average void fraction is defined as follows:

$$\alpha_a = \frac{\sum n_g}{N_a}, \tag{2}$$

where N_a is the total number of pixels in the inspection area, and n_g is the number of gas phase pixels. The inspection area was 1.4 mm × 1.4 mm (70 × 70 pixels) and was processed into a binary image of gas and liquid. From the definition of Equation (2), $\alpha_a = 1$ represents the case in which the entire inspection area is covered by the gas jet. In the case of no liquid droplet formation (u_0 = 13 m/s), α_a oscillated periodically between 1 and 0. With increasing gas jet velocity, the time intervals for the oscillations decreased. The existence of a certain period of liquid phase ($\alpha_a = 0$) indicates that the measurement is performed in the bubbling regime [6].

Note that for $u_0 \geq 50$ m/s, the void fractions exhibit values in the range of $\alpha_a > 0.8$ and $0.2 < \alpha_a < 0.8$. The former represents the impingement of liquid droplets on the glass tube surface, and the latter is associated with the entrainment of ambient liquid sodium with a large quantity, as compared to liquid droplets. At the optical images of u_0 = 125 m/s, the latter was

observed during the periods of 25–50 ms and 120–170 ms, when pulsed void fractions appeared. For these time periods, a large quantity of ambient liquid sodium was entrained intensely into the gas jet and impinged on the glass tube. When, as in the bubbling regime, interface waves with irregular shapes are developed without producing droplets, the appearance of values in the range of $0.2 < \alpha_a < 0.8$ is reasonable.

For u_0 = 125 m/s, note that the time average void fraction, α_t, measured by the probe placed 2 mm from the forward stagnation point of the glass tube was 0.75, which was larger than the value of 0.65 that was temporally averaged from the time series of the area average void fraction obtained from the optical images. Since the liquid sodium impinging on the glass tube surface is decelerated compared to its velocity in the submerged gas jet just before striking the surface, the magnitude relation between the two values is reasonable. On the other hand, in the backward region, the temporally averaged area average void fraction, α_a, of 0.54 was found to agree well with the time average void fraction, α_t, of 0.56 as measured by the probe. As explained in our previous paper, both the gas and liquid phases at the non-wettable surface are smoothly released from the backward region to the wake region [8]. Therefore, the good agreement between the two values in the backward stagnation region is reasonable.

3.4. Droplet Size Distribution

Optical images with liquid droplets were selected for obtaining the droplet size distributions, and the diameters of approximately 800 to 1000 droplets were measured by counting the number of pixels corresponding to the droplet diameter. A pixel size of 20 μm was determined by a direct reading of the scale, which was placed on the glass tube surface. It was also confirmed that the distortion of images due to the curvature of the glass tube was negligible. The measurement error of droplet diameters is considered to be ±1 pixel (±20 μm). Note that when liquid droplets impinged on the glass tube surface, disintegration or coalescence of the droplets was observed in the vicinity of the surface. These droplets were

neglected in the measurement of droplet sizes.

In the present study, the apparent diameters, *d'*, of deformed droplets on the glass tube surface were measured. Thus, the data correction from *d'* to the true droplet diameter, *d*, was performed. The shape of the liquid droplets adhered on the surface can be classified into two patterns according to contact angle, θ, as shown in **Figure 7**. For $\theta < 90°$, a liquid droplet wets and spreads over the surface. Thus, the observed diameter corresponds to the bottom circle of the partial sphere that is largely deformed from a droplet. Considering that the volume of the partial sphere is equal to that of the true droplet, the diameter ratio between the partial sphere and the true droplet is expressed in terms of contact angle as follows:

$$\frac{d}{d'} = \frac{1}{2}\left[\frac{1-\cos\theta}{\sin\theta}\left\{3+\left(\frac{1-\cos\theta}{\sin\theta}\right)^2\right\}\right]^{1/3}. \quad (3)$$

In the same manner, for $\theta > 90°$, the diameter of the partial sphere deformed slightly from a droplet can be observed through the glass tube. Thus, the diameter ratio is derived as

$$\frac{d}{d'} = \frac{1}{2}\left[(1-\cos\theta)\left\{3\sin^2\theta+(1-\cos\theta)^2\right\}\right]^{1/3}. \quad (4)$$

The solid line shown in Figure 7 represents Equations (3) and (4). When the contact angle, θ, is less than 90°, the diameter ratio, *d/d'*, changes significantly, while for $\theta > 90°$, *d/d'* is approximately unity. Fortunately, in this low-temperature condition, liquid sodium is expected to exhibit the non-wetting property with respect to the glass tube.

Figure 8 shows the appearance of sodium droplets on the surface of the glass tube observed after the experiment. The picture was taken in the atmosphere after draining liquid sodium to a sodium storage tank and sufficiently cooling the sodium to room temperature. The solid sodium droplets remaining on the outer surface of the glass tube exhibit contact angles of approximately 120°. It is reasonable to consider that solid-state droplets remaining on the surface maintain the contact angles in liquid-state droplets. Therefore, the contact angle between liquid sodium droplets and the glass tube surface during the experiment was

determined to be 120°, and the droplet diameters were corrected to the true values using a diameter ratio of 0.945, as shown in Figure 7.

Figure 9 shows the droplet size distributions, $\Delta n/N$, obtained in each experiment for various gas jet velocities. Here, N is the total number of liquid droplets measured, and Δn is the number of liquid droplets included in every 56.7-μm increment (three-pixel increment with data correction). The figure shows that the number of smaller droplets increase with increasing gas jet velocity.

Drop sizes produced by atomizers were systematically examined by Nukiyama and Tanasawa [7]. They proposed the following Nukiyama–Tanasawa distribution function:

$$f(d) = Ad^{\alpha} \exp(-Bd^{\beta}), \tag{5}$$

$$A = \frac{\beta B^{(\alpha+1)/\beta}}{\Gamma\{(\alpha+1)/\beta\}}, \tag{6}$$

$$B = \left[\frac{1}{d_s} \cdot \frac{\Gamma\{(\alpha+4)/\beta\}}{\Gamma\{(\alpha+3)/\beta\}}\right]^{\beta} \tag{7}$$

or

$$B = \left[\frac{1}{d_m} \cdot \frac{\Gamma\{(\alpha+2)/\beta\}}{\Gamma\{(\alpha+1)/\beta\}}\right]^{\beta}, \tag{8}$$

where Γ is the gamma function, α and β are empirical constants, and d_s and d_m are the Sauter mean diameter and arithmetic mean diameter of liquid droplets, respectively. After an extensive study on liquid atomization making use of several types of atomizers, they concluded that β is independent of the type of atomizer and is always unity and that α = 2 for airblast atomizers, which atomize liquid by causing the interaction of high-velocity gas and liquid. Their conclusions on airblast atomizers are also used in the present study because of the experimental similarities, namely, the mass flow rate of gas is sufficiently larger than that of liquid and the velocity of gas flow is considerably high. Therefore, α = 2 and β = 1 are substituted into Equations (5) through (8), to obtain

$$f(d) = \frac{125}{2d_s^{\,3}} d^2 \exp\left(-\frac{5}{d_s} d\right), \tag{9}$$

and

$$f(d) = \frac{27}{2d_m^{\,3}} d^2 \exp\left(-\frac{3}{d_m} d\right) \tag{10}$$

The broken line and the solid line in Figure 9 represent Equations (9) and (10), respectively. For u_0 = 50 m/s, the two lines overlap, whereas for u_0 = 75 and 125 m/s, Equations (9) and (10) represent different functions. The maximum and average deviations between the measured data and Equation (9) are 0.23 and 0.03, respectively, while those from Equation (10) are 0.13 and 0.02, respectively. Therefore, the selection of d_m as the characteristic diameter results in better agreement with the experimental data. This may be primarily attributed to the fact that large droplets governing d_s were limited in the present study. Note that although the comparison was in the bubbling regime, the good agreement of the present data with the Nukiyama–Tanasawa distribution function is a promising step toward the modeling of sodium–water reaction jets.

3.5. Mean Droplet Diameter

Epstein *et al.* measured the diameters of droplets produced by underexpanded gas jets slightly submerged in a water pool as a basic study on the sodium–water reaction [5]. They considered that the slightly submerged gas jet causes atomization in the almost same manner as in deeply submerged gas jets. The normalized Sauter mean droplet diameters were correlated in terms of the Weber number based on the gas jet diameter and velocity at the end of the external expansion zone described in their paper. In the present study, conducted in the low gas jet velocities up to 125 m/s, most of the sodium droplets were confirmed to be produced in the vicinity of the gas nozzle, as explained in Figures 3 and 5. Therefore, in the same manner as in the experiment for atomizing gas velocities of up to 120 m/s conducted by

Rizk and Lefebvre for gas turbines, the nozzle diameter, d_0, and the gas jet velocity at the nozzle exit, u_0, were used as the characteristic length and the characteristic velocity, respectively. Then the correlation proposed by Epstein *et al.* is converted into the following relationship:

$$\frac{d_s}{d_0} = 0.38\left(\frac{\sigma}{u_0^{\,2}\rho_g d_0}\right)^{0.4}, \qquad (11)$$

where σ is surface tension [N/m] and ρ_g is density of gas [kg/m^3] [9]. The normalized Sauter mean diameter is expressed as a function of Weber number defined by the gas jet condition at the nozzle exit.

Figure 10 shows the measured mean droplet diameters in the coordinate system suggested by Equation (11). The plotted values were obtained using the physical properties for liquid sodium and argon gas at 120°C: σ = 0.195 N/m and ρ_g = 1.217 kg/m^3. As shown in the figure, good agreement between Equation (11) and the present data on Sauter mean diameter is obtained. This indicates that Equation (11), which was obtained from a water experiment, is applicable to liquid sodium atomization, which has a surface tension that is approximately 3 times higher than that of water.

Similarly, the data for the arithmetic mean diameter, d_m, were also plotted in the figure. An empirical equation for d_m was then derived by the least squares method:

$$\frac{d_m}{d_0} = 0.17\left(\frac{\sigma}{u_0^{\,2}\rho_g d_0}\right)^{0.38}. \qquad (12)$$

Coupling of Equations (10) and (12) can predict the distribution of liquid droplets formed within a submerged gas jet under the present experimental condition.

4. Conclusions

Entrainment behaviors of liquid sodium into inert gas jets, which were submerged in

liquid sodium under the condition of the bubbling regime, were experimentally investigated. The following conclusions were obtained.

1. Gas jet behaviors impinging on a single tube submerged in liquid sodium were successfully visualized using an endoscope and a Pyrex glass tube.
2. Most of the sodium droplets are produced intermittently at the near region from the nozzle exit when the relative velocity between the gas jet and the ambient liquid reaches a maximum value corresponding to the characteristics in the bubbling regime.
3. Droplet size distributions of entrained liquid sodium agree well with the Nukiyama–Tanasawa distribution function, i.e., Equation (10), which uses arithmetic mean diameter as the characteristic diameter.
4. Sauter mean diameters and arithmetic mean diameters for entrained sodium droplets can be predicted by Equations (11) and (12), which take the nozzle diameter and the gas jet velocity at the nozzle exit as a characteristic length and a characteristic velocity, respectively.

Nomenclature

A, B	:	experimental constants [-]
d	:	droplet diameter [m]
d'	:	apparent diameter [m]
d_0	:	nozzle-hole diameter [m]
d_m	:	arithmetic mean diameter [m]
d_s	:	Sauter mean diameter [m]
f	:	distribution function [-]
N	:	number of measured droplets [-]
N_a	:	number of pixels in the inspection area [-]
n_g	:	number of pixels of the gas phase [-]

Δn : number of droplets in a particular range of diameter [-]

Q : volume flow rate [m^3/s]

u_0 : gas jet velocity at the nozzle exit [m/s]

Greek Letters

α, β : experimental constants [-]

α_a : area average void fraction [-]

α_t : time average void fraction [-]

Γ : gamma function [-]

θ : contact angle [degrees]

ρ_g : density of gas [kg/m^3]

σ : surface tension [N/m]

References

[1] E. Loth, G.M. Feath, Structure of underexpanded round air jets submerged in water, *Int. J. Multiphase Flow* 15 (1989), pp. 589–603.

[2] E. Loth, G.M. Feath, Structure of plane underexpanded air jets into water, *AIChE Journal* 36[6] (1990), pp. 818–826.

[3] S. Someya, M. Uchida, Y. Li, H. Ohshima, K. Okamoto, Entrained droplets in underexpanded gas jet in water, *J. Vis.* 14 (2011), pp. 225–236.

[4] R. Bell, B.E. Boyce, J.G. Collier, The structure of a submerged impinging gas jet, *J. Br. Nucl. Energy Soc.* 11 (1972), pp. 183–193.

[5] M. Epstein, H.K. Fauske, N. Yoshioka, Establishment of analytical model for peak temperature within a sodium-water reaction jet, (II); mean droplet size in a submerged gas jet, *J. Nucl. Sci. Tech.* 42[11] (2005), pp. 961–969.

[6] K. Mori, Y. Ozawa, M. Sano, Characterization of gas jet behavior at a submerged orifice in liquid metal, *Trans. ISIJ* 22 (1982), pp. 377–384.

[7] S. Nukiyama, Y. Tanasawa, Experiments on atomization of liquid, *JSME*, English translation by the Department of National Defence, Canada 6 (1950), pp. 1938–1940.

[8] H. Kudoh, D. Zhao, K. Sugiyama, T. Narabayashi, H. Ohshima, A. Kurihara, Void fraction distributions of inert gas jets across a single cylinder with non-wetting surface in liquid sodium, *J. Nucl. Sci. Tech.* 49[12] (2012). (to appear in)

[9] N.K. Rizk, A.H. Lefebvre, Spray characteristics of plain-jet airblast atomizers, *Trans. ASME* 106 (1984), pp. 634–638.

Figure captions

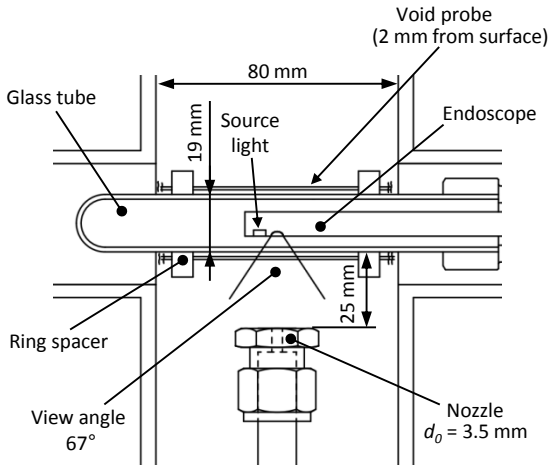

Figure 1 Schematic diagram of the test section

H. Kudoh:

Visualization on the Behavior of Inert Gas Jets Impinging on a Single Glass Tube Submerged in Liquid Sodium

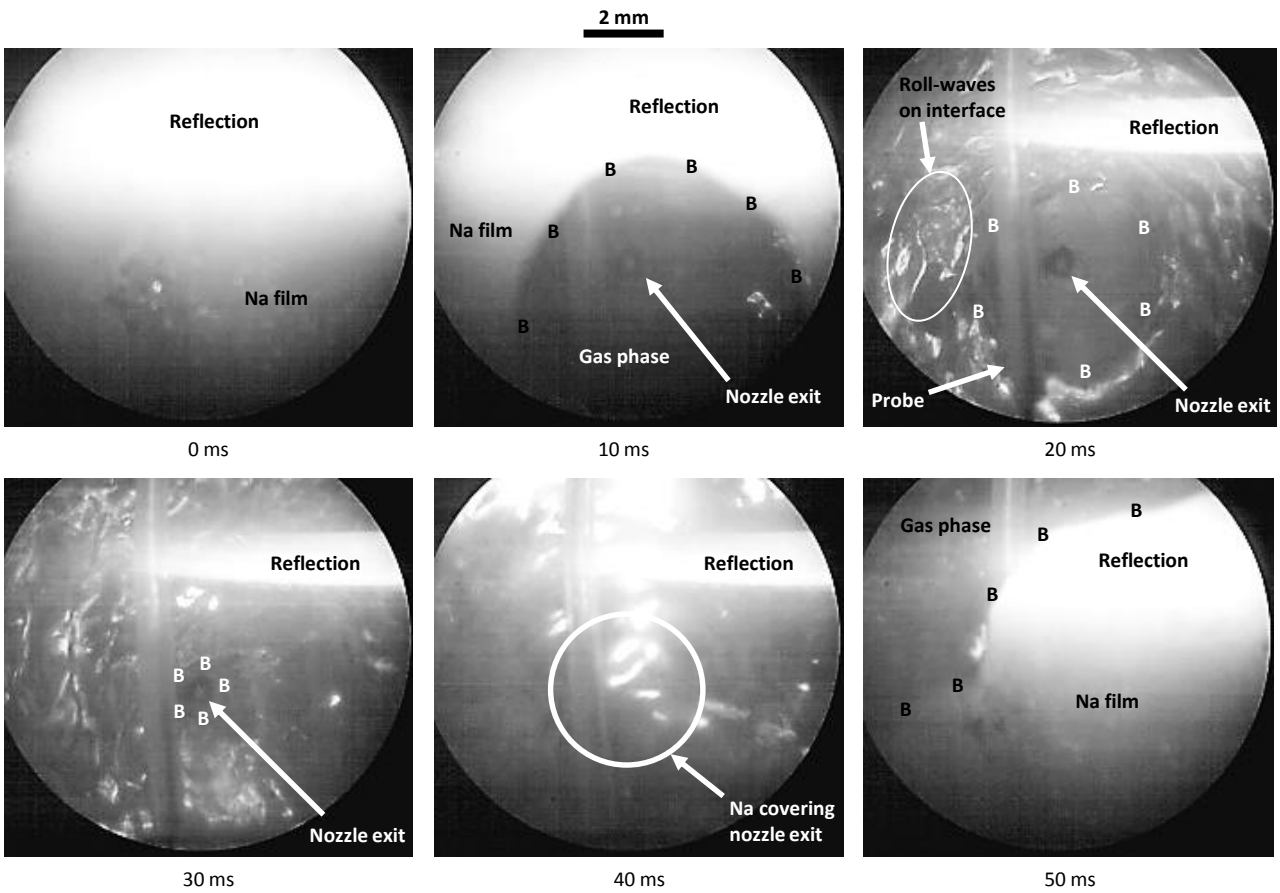

Figure 2 Optical images of the behavior of a gas jet submerged in liquid sodium (u_0 = 13 m/s)

H. Kudoh:

Visualization on the Behavior of Inert Gas Jets Impinging on a Single Glass Tube Submerged in Liquid Sodium

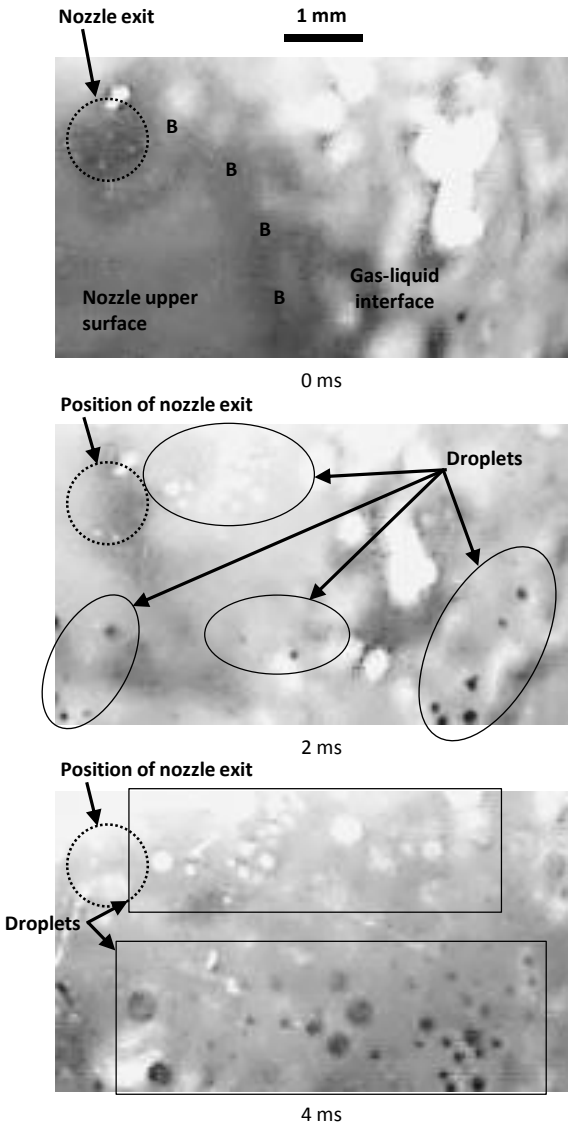

Figure 3 Droplet generation in the near region from the nozzle (u_0 = 75 m/s)

H. Kudoh:

Visualization on the Behavior of Inert Gas Jets Impinging on a Single Glass Tube Submerged in Liquid Sodium

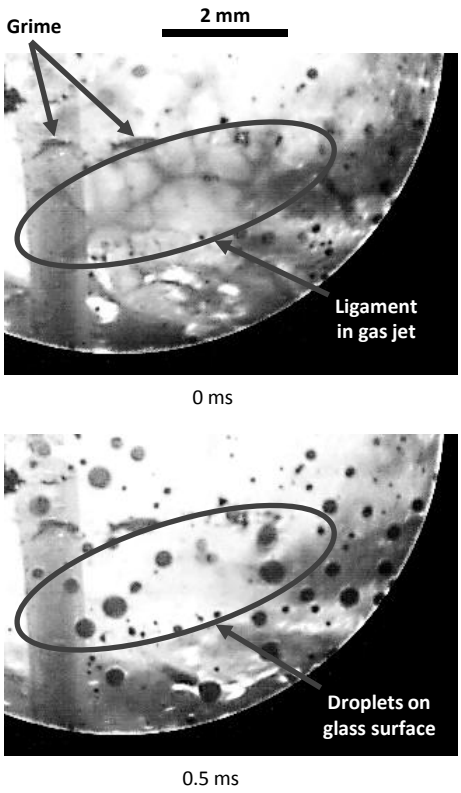

Figure 4 Droplet generation in the far region from the nozzle (u_0 = 75 m/s)

H. Kudoh:

Visualization on the Behavior of Inert Gas Jets Impinging on a Single Glass Tube Submerged in Liquid Sodium

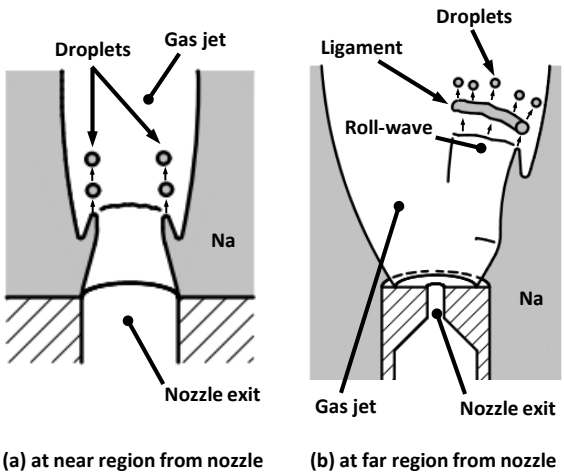

Figure 5 Illustration of droplet generation

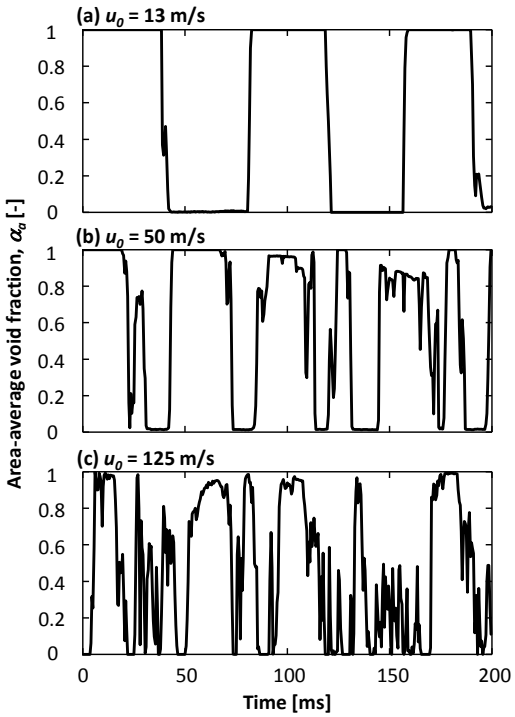

Figure 6 Time series of the area average void fraction

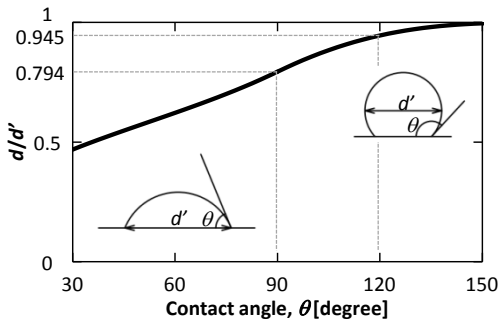

Figure 7 Correction of droplet diameter

H. Kudoh:

Visualization on the Behavior of Inert Gas Jets Impinging on a Single Glass Tube Submerged in Liquid Sodium

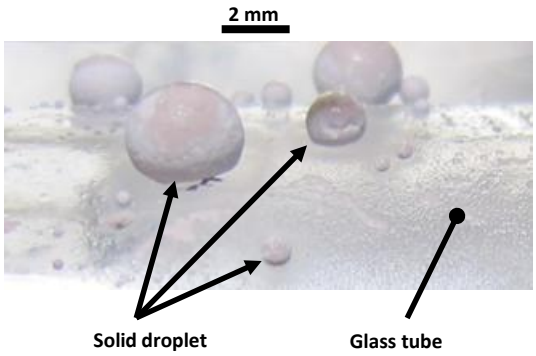

Figure 8 Solid droplets on the glass tube

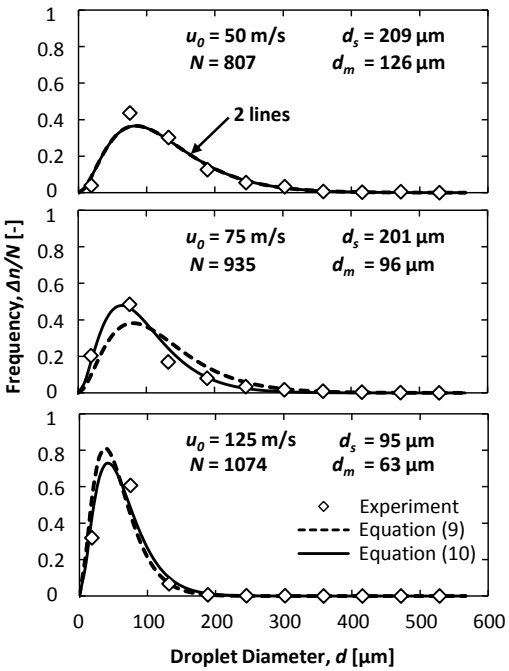

Figure 9 Droplet size distribution

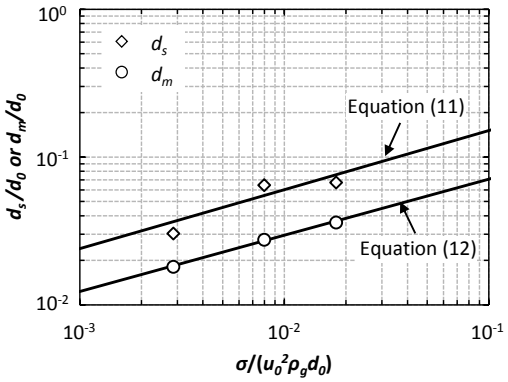

Figure 10 Correlation of mean droplet diameter

H. Kudoh:

Visualization on the Behavior of Inert Gas Jets Impinging on a Single Glass Tube Submerged in Liquid Sodium